Scissor-Jack-Damper Energy Dissipation System

Ani N. Şigaher,[a] M.EERI, and Michael C. Constantinou,[b] M.EERI

Installation of damping devices has been limited to diagonal or chevron brace configurations until the recent development of the toggle-brace configurations. These configurations magnify the effect of damping devices, thus facilitating their use in stiff framing systems. This paper introduces the scissor-jack-damper system that was developed as a variant of the toggle-brace-damper systems, with the added advantage of compactness. The effectiveness of the scissor-jack configuration is demonstrated through testing of a large-scale steel-framed model structure on an earthquake simulator. Experiments showed that despite the small size of the damping device considered, the scissor-jack system provided a significant amount of damping and substantially reduced the seismic response of the tested structure. Response history and simplified analyses produce results that are consistent with the experimental results. [DOI: 10.1193/1.1540999]

INTRODUCTION

The use of supplemental or damping devices to dissipate seismic energy in building and bridge structures has gained increasing interest in the past decade. These devices, commonly known as 'dampers,' exhibit either hysteretic behavior (e.g., yielding of metals, sliding friction) or viscoelastic/viscous behavior (e.g., fluid viscous dampers, solid and fluid viscoelastic dampers). The underlying objective of implementing energy dissipation devices in structural systems is to limit or eliminate damage to the structural frame by dissipating most of the earthquake-induced energy which would otherwise be absorbed by the load-bearing-system through inelastic deformations. Viscoelastic and viscous energy dissipation systems are also eminently suitable for wind vibration reduction. The interested reader is referred to the following for a review of this technology: Applied Technology Council (ATC) (1997), Soong and Dargush (1997), Constantinou et al. (1998), and Hanson and Soong (2001).

Today, many countries utilize various types of damping devices as protective systems to reduce wind and earthquake-induced vibrations in new and retrofit construction. In Japan, the majority of the applications utilize yielding steel devices and viscoelastic fluid or solid devices. In the United States, engineers have primarily used fluid viscous devices. In these applications, damping devices have either been installed in-line with diagonal bracing or as horizontal elements atop chevron bracing. The popularity of these

[a] Graduate Research Assistant, Department of Civil, Structural and Environmental Engineering, University at Buffalo, State University of New York, Buffalo, NY 14260

[b] Professor and Chair, Department of Civil, Structural and Environmental Engineering, University at Buffalo, State University of New York, Buffalo, NY 14260

configurations is based on the engineers' familiarity with such bracing systems and the fact that all experimental research studies have utilized only these two configurations for energy dissipation systems.

Exception to the rule of use of diagonal or chevron bracing configurations for damping systems has been the recent construction of two 37-story and one 38-story buildings in the United States utilizing the toggle-brace configuration. As the name implies, this configuration is based on the toggle mechanism, which magnifies the damper displacement for a given interstory drift. This amplification results in a reduction in the required damping force, and reduction in the damper volume, which may lead to reduction of damper cost. The damper force output is magnified through the same mechanism and delivered to the framing system. The toggle-brace configuration is suitable for applications of wind response reduction and of seismic hazard mitigation of stiff structures. A theoretical treatment of the system's behavior, along with experimental results confirming the validity of the concept and the developed theory, and a brief description of applications can be found in Constantinou et al. (2001).

An additional consideration related to the application of energy dissipation systems is that in many cases the energy dissipation assemblies occupy entire bays in frames and often violate architectural requirements such as open space and unobstructed view. With this intent, the scissor-jack-damper system was developed as a variant of the toggle-brace-damper system. The system combines the displacement magnification feature with small size, which is achieved through compactness and near-vertical installation.

This paper presents the concept underlying the scissor-jack-damper configuration and verifies the theory via experimental results. The experimental study includes earthquake simulator testing of a half-scale steel model structure equipped with fluid viscous dampers. Parts of the work described in this paper have been previously presented or briefly described by the authors and coworkers (Whittaker and Constantinou 1999a, 1999b, 2000; Constantinou et al. 2000; Constantinou 2000; Constantinou and Şigaher 2000). The scissor-jack system is also briefly described in the recent EERI monograph of Hanson and Soong (2001). However, this paper represents the first detailed treatment of the scissor-jack-damper system and the related experimental results, which represent part of the doctoral dissertation of the first author.

SCISSOR-JACK-DAMPER THEORY

The scissor-jack-damper system is best explained by first reviewing the conventional diagonal and chevron brace configurations, in which the displacement of the energy dissipation devices is either less than (case of diagonal brace) or equal to (case of chevron brace) the drift of the story at which the devices are installed. If u and u_D denote the interstory drift and the damper relative displacement, respectively, then

$$u_D = f \cdot u \tag{1}$$

where f = magnification factor. For the chevron brace configuration, $f = 1.0$; for the diagonal configuration $f = \cos \theta$, where θ = angle of inclination of the damper with respect to the horizontal axis. The force F_D along the damper axis is similarly related to F, the horizontal component of the damper force exerted on the frame, through
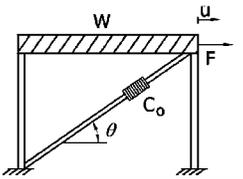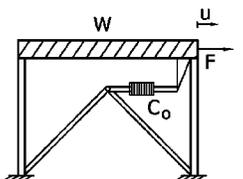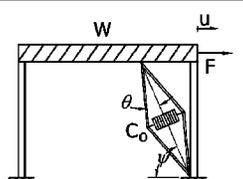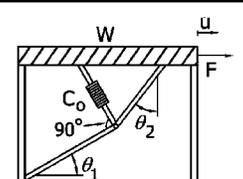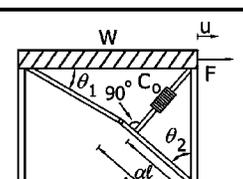
Diagonal		$f = cos\theta$	$\theta = 37^{\circ}$ $f = 0.80$ $\beta = 0.03$
Chevron		$f = 1.00$	$f = 1.00$ $\beta = 0.05$
Scissor-Jack		$f = \dfrac{cos\psi}{tan\theta}$	$\theta = 9^{\circ}, \psi = 70^{\circ}$ $f = 2.16$ $\beta = 0.23$
Upper Toggle		$f = \dfrac{sin\theta_2}{cos(\theta_1 + \theta_2)} + sin\theta_1$	$\theta_1 = 31.9^{\circ}, \theta_2 = 43.2^{\circ}$ $f = 3.191$ $\beta = 0.509$
Reverse Toggle		$f = \dfrac{\alpha \, cos\theta_1}{cos(\theta_1 + \theta_2)} - cos\theta_2$	$\theta_1 = 30^{\circ}, \theta_2 = 49^{\circ}, \alpha = 0.7$ $f = 2.521$ $\beta = 0.318$

Figure 1. Illustration of diagonal, chevron brace, scissor-jack-damper, and toggle-brace-damper configurations, magnification factors, and damping ratios of a single-story structure with linear fluid viscous devices.

$$F = f \cdot F_D \qquad (2)$$

Figure 1 illustrates a single-story structure with diagonal and chevron brace configurations. Also shown in the figure are the force, F, and the interstory drift, u. Consider that this single-story structure has an effective weight, W, and a fundamental period under elastic conditions, T, and that it is equipped with a linear fluid viscous damper for which

$$F_D = C_o \cdot \dot{u}_D \qquad (3)$$

where C_o=damping coefficient, and $\dot{u}_D$=relative velocity between the ends of the damper along its axis. The damping force F, exerted on the frame by the damper assembly is given by

$$F = C_o \cdot f^2 \cdot \dot{u} \tag{4}$$

in which $\dot{u}$=interstory velocity. It follows that the damping ratio of a single-story frame with a linear fluid viscous device can be written as

$$\beta = \frac{C_o \cdot f^2 \cdot g \cdot T}{4 \cdot \pi \cdot W} \tag{5}$$

It is essential to realize the effect of the magnification factor on the damping ratio. As Equation 5 suggests, the damping ratio varies proportionally with the square of the magnification factor. In the two conventional configurations in Figure 1, a damper designed to provide a damping ratio of 5 percent of critical when installed horizontally (chevron brace), will provide a damping ratio of 3.2 percent of critical in the diagonal configuration.

In contrast to the familiar diagonal and chevron brace configurations, the scissor-jack configuration can achieve magnification factors substantially greater than unity. This is also true for the toggle-brace-damper systems. Figure 1 also illustrates the scissor-jack-damper and toggle-brace-damper systems as implemented in a single-story frame. These systems make use of shallow trusses that amplify the effect of the interstory drift on the damper displacement and also amplify the small damper force and deliver it to the structural frame. The expression for the magnification factor, f, under the assumption of small rotations, and its value for a typical geometry are also given in Figure 1. A substantial increase in the damping ratio with respect to that provided by conventional damper configurations demonstrates the efficacy of these systems.

The presence of the magnifying mechanism in the scissor-jack system extends the utility of fluid viscous devices to cases of small interstory drifts and velocities, which are typical of stiff structural systems under seismic excitation and structures subjected to wind load. Fluid viscous devices require special detailing when operating at small stroke. This results in an increased volume of the device and, accordingly, cost. In addition, in stiff structural systems, the required damping forces are large, leading to a further increase in the cost of the energy dissipation system. These damper configurations, therefore, may lead to cost savings, provided that the cost of the support framing is not substantially greater than the cost of the framing that would be required to support the dampers in conventional configurations. Moreover, the scissor-jack system may be configured to allow for open space, minimal obstruction of view and slender configuration, features that are often desired by architects.

The scissor-jack damping system may be installed in a variety of configurations as shown in Figure 2.
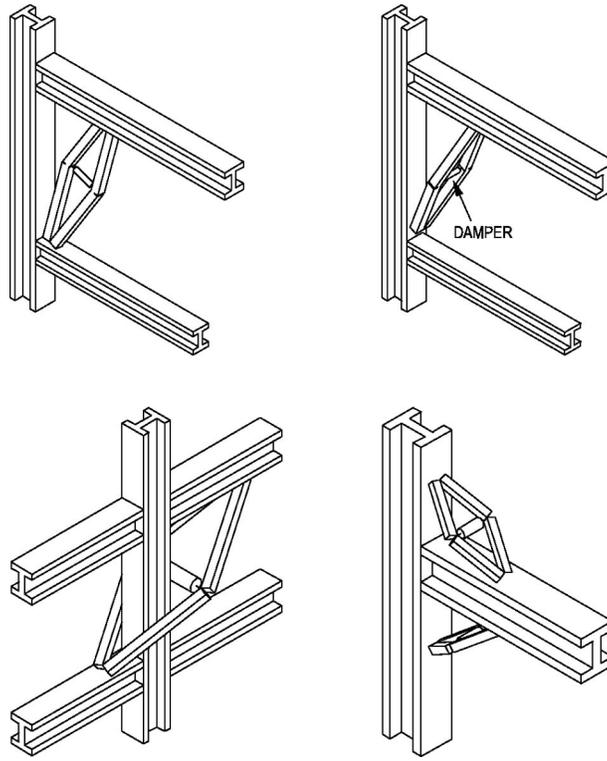
Figure 2. Possible installation configurations of a scissor-jack-damping system.

MAGNIFICATION FACTOR AND FORCES IN SCISSOR-JACK SYSTEM

The effectiveness of the scissor-jack configuration is based on the magnification factor, f, defined as the ratio of damper displacement, u_D, to the interstory drift, u. Figure 3 presents an analysis of the movement of a single-story frame with a scissor-jack system. The magnification factor is

$$f = \frac{u_D}{u} = \frac{|\overline{A'B'} - \overline{AB}|}{u} \tag{6}$$

where $\overline{AB}$ and $\overline{A'B'}$ denote the initial and the deformed lengths of the damper, respectively.

It should be noted that the deformed configuration of Figure 3 does not take into account any deformations in the frame (only rigid body motion is considered) and any reduction in height due to column rotation. The latter has negligible effect on the magnification factor for typical values of interstory drift and for low-rise structures. The frame deformations, on the other hand, may have notable effect on the magnification factor. As an example, consider that the beam in Figure 3 is simply connected to the column on the left and rigidly connected to the column on the right. Upon an interstory drift
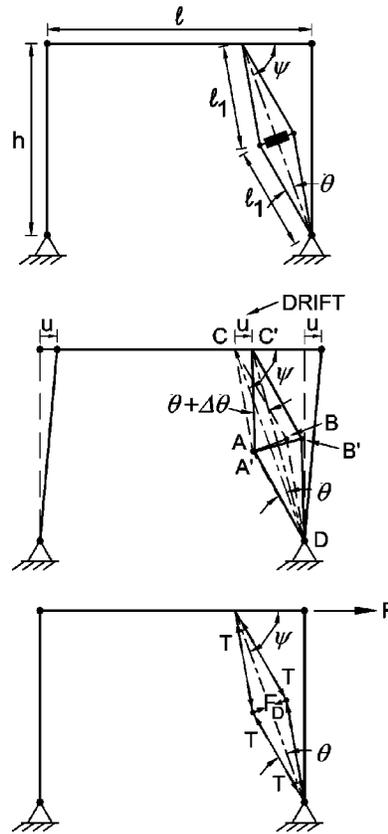
Figure 3. Analysis of scissor-jack movement and analysis of forces.

towards the right, the beam will deflect upwards, causing a decrease in the damper deformation and thus, in the magnification factor. The opposite will occur when the beam-to-column connections are reversed. This type of amplification/deamplification of the magnification factor will depend on the relative stiffnesses of the beam and the column, and the position of the point of connection of the scissor-jack on the beam. Additionally, the displacements due to the forces in the damper and in the scissor-braces (i.e., displacements due to finite stiffness of the scissor-braces) will reduce the magnification factor, regardless of the structural system configuration. A treatment of the effect of the deformations in the frame and in the damper assembly, on the behavior of the frame will be presented in sections that follow.

Based on rigid body kinematics, the damper displacement may be expressed as

$$u_D = |\overline{A'B'} - \overline{AB}| = \pm 2 \cdot \ell_1 \cdot [\sin(\theta \pm \Delta\theta) - \sin\theta] \tag{7}$$

where $\Delta\theta$ = angle of rotation of the scissor-braces. Preservation of lengths between points C and D requires that
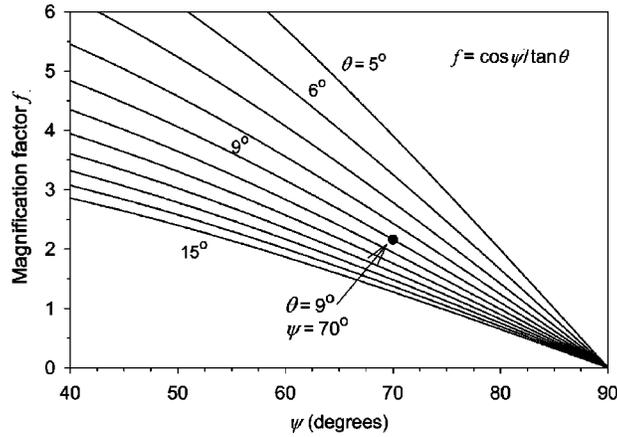
Figure 4. Dependency of the magnification factor on the scissor-jack geometry.

$$2\cdot\ell_1\cdot\cos(\theta\pm\Delta\theta)=2\cdot\ell_1\cdot\cos\theta\mp u\cdot\cos\psi \tag{8}$$

Utilizing Equations 7 and 8, the damper displacement can be written as

$$u_D=\pm2\cdot\ell_1\cdot\left[\sin\left(\cos^{-1}\left\{\cos\theta\mp\frac{\cos\psi}{2\cdot\ell_1}\cdot u\right\}\right)-\sin\theta\right] \tag{9}$$

where in Equations 7 to 9, positive signs hold for drift towards the right (u and $\Delta\theta$ as shown in Figure 3) and for damper extension ($u_D>0$). For drift towards the left, these equations are valid with negative signs.

Equation 9 may be used to calculate the damper displacement given a value of drift, provided the latter is small. However, the equation cannot be solved for the ratio of two displacements, which is of much practical value. Realizing that for most applications $\Delta\theta$ is very small, Equations 7 and 8 may be significantly simplified to easily yield the magnification factor

$$f=\frac{\cos\psi}{\tan\theta} \tag{10}$$

It can be shown that Equations 1 and 10 provide a very good approximation to the exact damper deformation (Equation 9) for $\Delta\theta\leqslant0.2\theta$. Moreover, Equation 10 provides insight into the major factors affecting the performance of the scissor-jack configuration.

The dependence of the magnification factor, f, on angles θ and ψ is illustrated in Figure 4. As the figure suggests, the magnification factor assumes very large values as θ approaches 0°; but this has no meaning since the scissors tend to act as a single brace inclined at angle ψ. Rather, when designing such systems, emphasis should be placed on the fact that the magnification factor should have minimal sensitivity to small changes

in geometry. A typical geometry is shown in Figures 1 and 4, which is representative of the tested scissor-jack-damper system. Practical values of the magnification factor lie in the range 2 to 5.

The forces that act on the scissor-jack and on the single-story frame are also shown in Figure 3. It should be noted that the frame shown is a mechanism such that force F represents the component of the inertia force that is balanced by forces from the damping system. Considering equilibrium in the original, undeformed configuration reveals the forces that develop in the scissor-braces as

$$T = \frac{1}{2 \cdot \sin \theta} \cdot F_D \tag{11}$$

where T and F_D denote the forces in the brace and damper, respectively. Note that the forces T are greater than the force F_D by a factor of $1/2 \cdot \sin \theta$ due to the shallow truss configuration of the scissor-braces. The resultant of the horizontal component of forces T equals force F, that is,

$$F = 2 \cdot T \cdot \cos \theta \cdot \cos \psi \tag{12}$$

Equation 12 together with Equation 11, result in Equation 2. That is, the magnification factor can be written as

$$f = \frac{u_D}{u} = \frac{F}{F_D} \tag{13}$$

which proves the accuracy of the analysis presented.

DAMPING RATIO AND PERIOD OF STRUCTURE WITH DAMPING SYSTEM

The addition of energy dissipation devices to a building results in a nonclassically damped structure even if the structure itself has classical damping. Exact methods to determine the dynamic properties (e.g., frequencies of free vibration, mode shapes, and damping ratios) of the damped structure are available, but may become involved since they necessitate complex eigenvalue analysis. The interested reader is referred to Veletsos and Ventura (1986) for a comprehensive treatment of the complex eigenvalue problem, and Constantinou and Symans (1992) for an illustration of the exact analysis for the case of linear viscous and viscoelastic fluid dampers.

Moreover, the addition of energy dissipation devices to a building results in an increase in stiffness and a reduction in period. This phenomenon is well understood for devices with viscoelastic behavior (e.g., see Soong and Dargush 1997, Constantinou et al. 1998, and Hanson and Soong 2001).

An alternative to the exact methods is the use of approximate methods of analysis based on energy principles. Such methods are very simple to apply and, accordingly, have been utilized in analysis and design provisions and guidelines (ATC 1997, FEMA 2000). The approximate methods of analysis typically provide results of acceptable accuracy when complete vertical distributions of damping devices are used.

The energy dissipation assembly exhibits, in general, viscoelastic behavior depending on the geometry, stiffness and damping of the elements comprising the assembly. In the case of a linear viscous damper with a damper coefficient, C_o, the assembly can be represented by a spring in series with the viscous damper. The behavior is then best described by the Maxwell viscoelastic model for which the horizontal force, F_j, exerted on the frame at story j by the energy dissipation system is described by

$$F_j + \tau_j \cdot \dot{F}_j = C_{oj} \cdot f_j^2 \cdot \dot{u}_j \tag{14}$$

where $\dot{u}_j$ is the interstory drift velocity at story j, τ_j is the relaxation time that is the ratio of the damping coefficient to the stiffness of the damping assembly at story j, and f_j is the magnification factor at story j. The interested reader is referred to Hanson and Soong (2001) for a treatment of the issue of the effect of the flexibility of the energy dissipation assembly. Herein it is of importance to emphasize that the energy dissipation assembly includes, in addition to the damper-bracing assembly, the frame to which all these are connected. For example, significant flexibility will result from frame deformations in structures with scissor-jack-damper systems when installed as shown in Figure 1. This is also true for structures with toggle-brace-damper systems as demonstrated by Constantinou et al. (2001). Actually, the development of the reverse toggle-brace-damper system has been motivated by a desire to minimize the flexibility of the energy dissipation assembly.

The force F may be alternatively, in a further simplification, described using the Kelvin viscoelastic model as a function of relative displacement u, and relative velocity $\dot{u}$, as

$$F_j = k_j'(\omega) \cdot f_j^2 \cdot u_j + c_j'(\omega) \cdot f_j^2 \cdot \dot{u}_j \tag{15}$$

where k_j' and c_j' are, respectively, the storage stiffness and damping coefficient of the energy dissipation system at story j, which are given by

$$k_j'(\omega) = \frac{C_{oj} \cdot \tau_j \cdot \omega^2}{1 + \tau_j^2 \cdot \omega^2} \quad \text{and} \quad c_j'(\omega) = \frac{C_{oj}}{1 + \tau_j^2 \cdot \omega^2} \tag{16}$$

and ω is the frequency of free vibration of the damped structure. It should be noted that for infinitely stiff bracing ($\tau_j = 0$), the energy dissipation system behaves as a pure viscous system and Equations 14 to 16 reduce to Equation 4.

The approximate energy method starts with the assumption that the frequencies and mode shapes of the nonclassically damped structure are identical to those of the undamped structure with the added effect of storage stiffness, but not of damping, from the energy dissipation assembly. Thus, the frequencies and mode shapes can be determined from standard eigenvalue analysis. Assuming that the structure undergoes vibration in the kth mode with period T_k (or with frequency of vibration in the kth mode equal to ω_k), the damping ratio at the jth story may be expressed (Constantinou and Symans 1992, ATC 1997, FEMA 2000) as

$$\beta_k = \frac{g}{4 \cdot \pi} \cdot \frac{T_k \cdot \Sigma_j c_j'(\omega_k) \cdot f_j^2 \cdot \phi_{rj}^2}{\Sigma_i W_i \cdot \phi_i^2} \tag{17}$$

where ϕ_{rj} is the kth modal interstory drift of the jth story; W_i=lumped weight at the ith level; and ϕ_i=modal displacement of level i in the kth mode of vibration. Summation j extends over all stories and summation i extends over all lumped weights. Note that f_j is equal to $\cos \theta_j$ (θ_j=inclination angle of the dampers) for devices installed diagonally; is unity for the case of chevron brace configuration of Figure 1; and $\cos \psi_j / \tan \theta_j$ (refer to Figure 1 for angles ψ_j and θ_j) for the scissor-jack system. For a single-story structure, $\phi_{rj} = \phi_i = 1$, $i = j = 1$, and Equation 17 simplifies, for the case of rigid energy dissipation assembly, to Equation 5.

Within the context of approximate methods of analysis (as, for example, those described in the 2000 edition of the *NEHRP Recommended Provisions*), the mode shapes may be assumed or calculated for the undamped structure without the effect of the storage stiffness resulting from the viscoelastic nature of the energy dissipation assembly. Such an approximation produces acceptable results when the distribution of damping devices is complete over the building height. In such cases, it is of interest to develop a simple approximate method of estimating the periods of the damped structure. In arriving at an approximate method, we recognize that

$$T_k' = 2 \cdot \pi \cdot \left[\frac{\Sigma_i W_i \cdot \phi_i^2}{g \cdot \Sigma_j K_j \cdot \phi_{rj}^2} \right]^{1/2} \tag{18}$$

where T_k' is the kth mode period of the undamped structure and K_j is the horizontal stiffness of story j. Moreover,

$$T_k = 2 \cdot \pi \cdot \left[\frac{\Sigma_i W_i \cdot \phi_i^2}{g \cdot \Sigma_j (K_j + c_j' \cdot \tau_j \cdot \omega_k^2 \cdot f_j^2) \cdot \phi_{rj}^2} \right]^{1/2} \tag{19}$$

Equations 17 to 19 may be combined to arrive at the following equation provided that the mode shape is the same for the undamped and the damped structure:

$$T_k = T_k' \cdot \left[1 - \frac{4 \cdot \pi \cdot \tau \cdot \beta_k}{T_k} \right]^{1/2} \tag{20}$$

where parameter τ was assumed to be the same for all stories of the structure, or τ is an average representative value for all stories. Equation 20 is implicit in the calculation of period T_k, requiring an iterative procedure to solve. However, given the approximate nature of the calculation, the following equation, representing the first iteration result, may be used.

$$T_k \approx T_k' \cdot \left[1 - \frac{4 \cdot \pi \cdot \tau \cdot \beta_k}{T_k'} \right]^{1/2} \tag{21}$$

EXPERIMENTAL PROGRAM

The scissor-jack-damper system was first tested in a frame connected to a strong floor and subjected to an imposed displacement history, and then in a model structure on the earthquake simulator at the University at Buffalo. The model was the half-scale steel-framed structure, which was previously utilized for testing of the toggle-brace-damper system (Constantinou et al. 2001). The model structure consisted of two identical frames that could be tested individually on the strong floor or together on the earthquake simulator with an added mass on the top of the frames. Figure 5 illustrates one of the two tested frames with the scissor-jack-damper system. A view of the structure on the earthquake simulator is presented in Figure 6. The model features the following characteristics:

1. Beam-to-column connections of the model frames were easily convertible from simple to rigid, by bolting stiffened angles to the flanges of the beam and column (see Figure 5). This enabled testing with one rigid and one simple connection per frame (referred to as rigid-simple or simple-rigid configurations) and with two rigid configurations per frame (rigid-rigid configuration). The rigid-simple, simple-rigid, and rigid-rigid configurations were tested in the strong floor experiments, whereas the earthquake simulator testing included only rigid-simple and simple-rigid configurations.

2. The scissor-braces were connected to the frame (scissors-to-beam and scissors-to-column connections) utilizing plates, which were designed to undergo mainly rotation. As shown in the detail of Figure 5, these plates were designed with sufficient length to prevent inelastic action. The damper-to-brace connections were designed as true pins to avoid transfer of bending forces to the damper. However, this was not fully accomplished because of tight pin configuration that exhibited considerable friction.

3. The concrete weight used for earthquake simulator testing comprised of two blocks weighing a total of 142.3 kN, and was secured atop the columns by way of simple connections. The center of mass of these blocks was 1,113 mm above the centerline of the beam.

4. A total of three viscous fluid dampers were utilized for the floor and earthquake simulator testing. Shown in Figure 7 are the peak force-peak velocity characteristics of the dampers (shown by triangular symbols), extracted from harmonic testing. It follows that for damper 1 (used in strong floor testing), the behavior is practically linear, which can be described by Equation 3 with C_o =25.8 N-s/mm for velocities up to 500 mm/s. Dampers 2 and 4 (used in earthquake simulator testing) exhibit linear behavior for velocities to 250 mm/s (with C_o=40.0 N-s/mm in Equation 3), after which the behavior deviates towards nonlinearity. For these dampers, the overall behavior can be described via F_D $=C_{No}\cdot\dot{u}_D{}^\alpha$, where C_{No}=137.3 N-(s/mm)$^\alpha$ and α=0.76. All dampers were of the run-through rod type construction, and had a length of 273 mm, a diameter of 44.5 mm, and a stroke of ±28.6 mm.
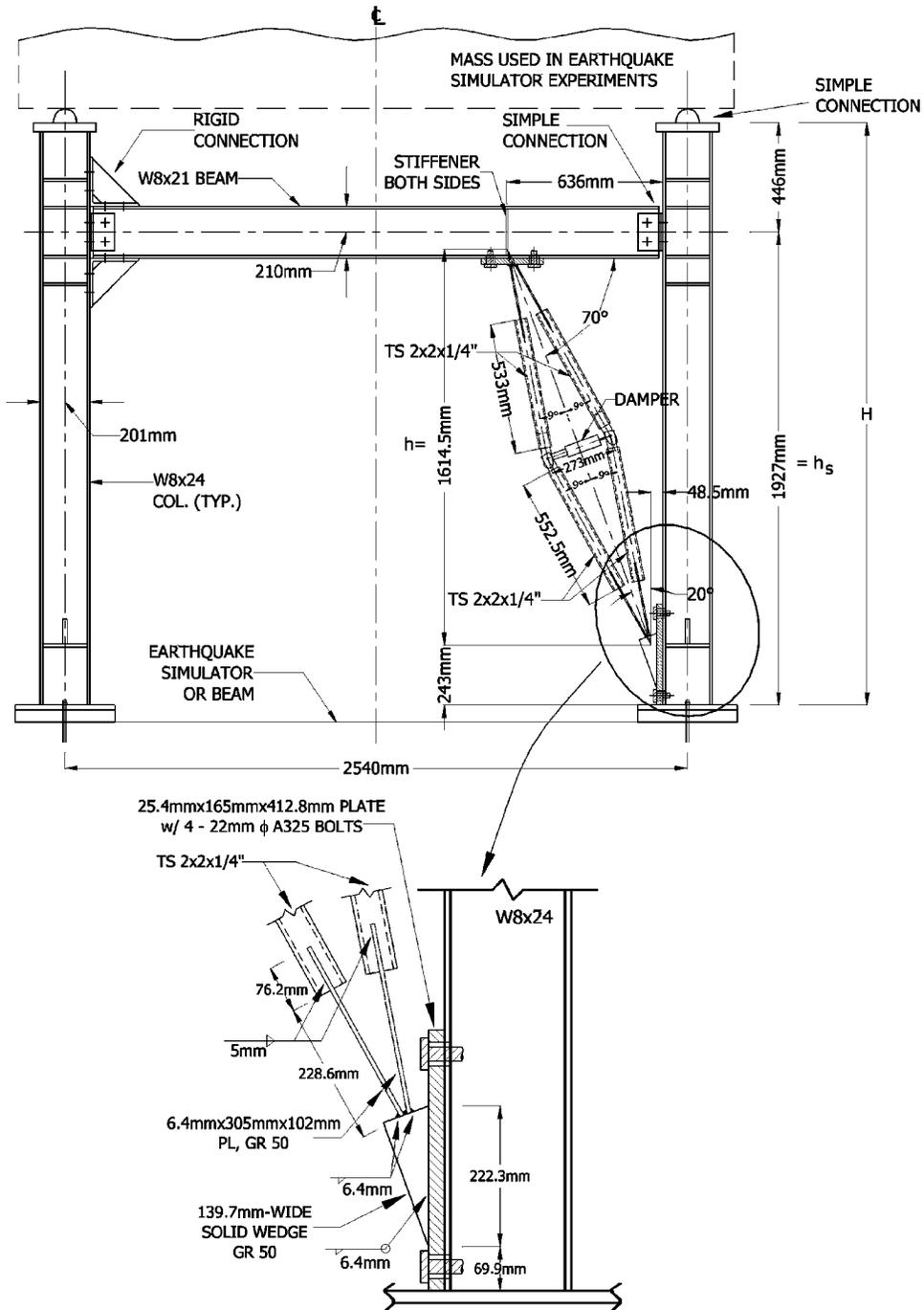
Figure 5. Tested scissor-jack-damper configuration.

Figure 6. Model with scissor-jack damping system on the Buffalo earthquake simulator.

TESTING OF FRAME WITH SCISSOR-JACK SYSTEM

One frame with the scissor-jack system (as shown in Figure 5), simply supported on a W21×50 beam that was bolted on the strong floor, was subjected to sinusoidal movement at various frequencies and amplitudes at its beam-to-column connection. The purpose of this testing was to confirm the predictions of the scissor-jack theory. Alternate types of beam-to-column connections were tested to observe the effect of the frame deformations on the magnification factor.

The behavior of the scissor-jack-damper system is illustrated in Figure 8 for the rigid-simple configuration of the frame. As noted earlier, this configuration, which is shown in Figure 5, produces the highest displacement magnification factor. The figure shows the relation between lateral force and lateral displacement of the frame, damper force and damper displacement, and damper displacement and lateral displacement of the frame (i.e., the magnification factor). Lateral displacement of the frame is the displacement of the beam-to-column joint (drift) and the lateral force is the force required to impose this displacement. In consistency with the earlier sign conventions, drift towards the right, resulting increase in damper length, and corresponding forces in the frame and the damper are taken positive.

The following observations can be made in the results of Figure 8:

1. The magnification factor attains its largest value under quasi-static conditions (0.01 Hz) when the viscous damping force is practically zero, and decreases with increasing frequency. This behavior is primarily the result of frame defor-
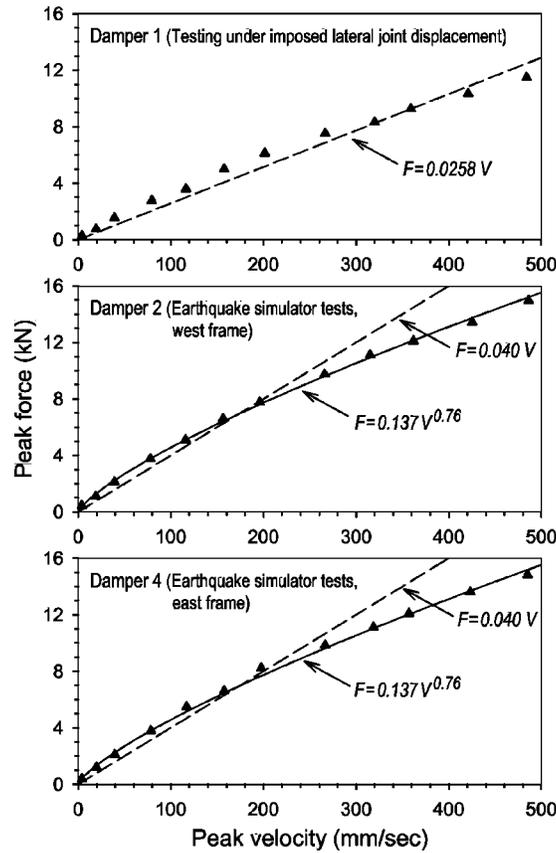
Figure 7. Peak force versus peak velocity relation of tested fluid viscous dampers.

mations under the action of forces in the scissor-jack system. Although the damper forces are low (force F_D in Figure 3), the resultant force on the frame (resultant of forces T in Figure 3 equals F_D/tan θ) is large (for the tested configuration, $\theta=9°$ so that F_D/tan $\theta=6.3\ F_D$) resulting in deflection of the beam.

2. Under quasi-static conditions, the magnification factor is higher than predicted by theory. For the tested frame, $u_D=f'\cdot u$, where $f'\approx f\cdot(h/h_s)$, and h/h_s is a factor accounting for the geometry in which the vertical projection, h, of the scissor-jack is less than the story height, h_s, where drift, u, occurs (see Figure 5). In this case, $h/h_s=0.838$ and $f\approx1.8$; whereas testing under quasi-static conditions revealed $f\approx2.9$ for negative drift (damper undergoes compression) and $f\approx2.5$ otherwise. The difference between the predicted and the observed magnification factors can be explained by the fact that with the beam-to-column connections configured as rigid-simple, part of the damper deformation is caused by vertical deflection of the beam (for either direction of drift)—a factor not accounted for in theoretical predictions. In addition, under negative drift (towards the left), as
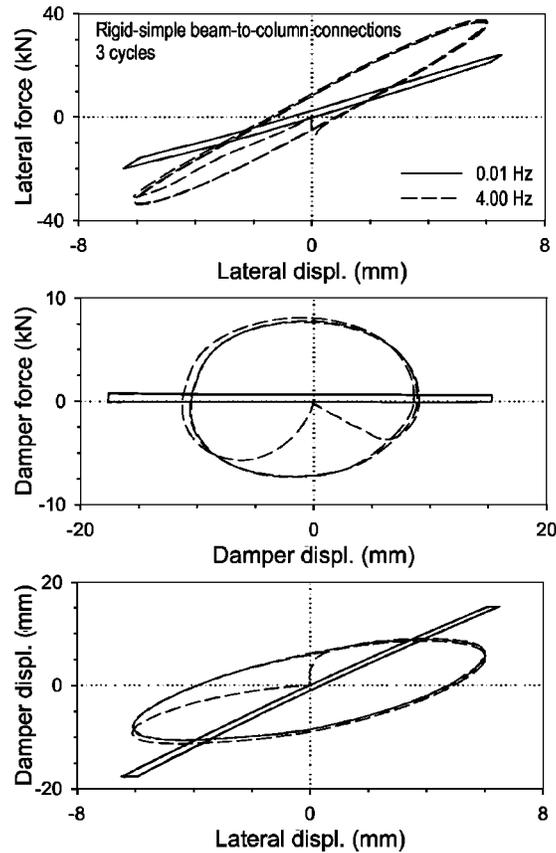
Figure 8. Recorded response of frame when subjected to lateral joint displacement.

the scissor-braces close, the angle θ decreases, causing an increase in the instantaneous magnification factor, which results in a larger value of f (see Figure 4).

3. Under dynamic conditions, for which considerable forces develop in the scissor-jack assembly, the magnification factor attains values of about 1.6 to 1.9, depending on whether the angle θ increases or decreases, respectively. The substantial reduction of the magnification factor from the values attained under quasi-static conditions is due to deformations of the energy dissipation assembly (primarily beam deflections) caused by the damping forces.

4. There is considerable increase in the effective stiffness of the frame when significant damping forces develop, as it is evident in the hysteresis loops of the top graph in Figure 8. These loops show a 60 percent increase in effective stiffness, which corresponds to about 25 percent increase in frequency. This is consistent with the predictions of Equation 21 and experimental results to be presented later in this paper.
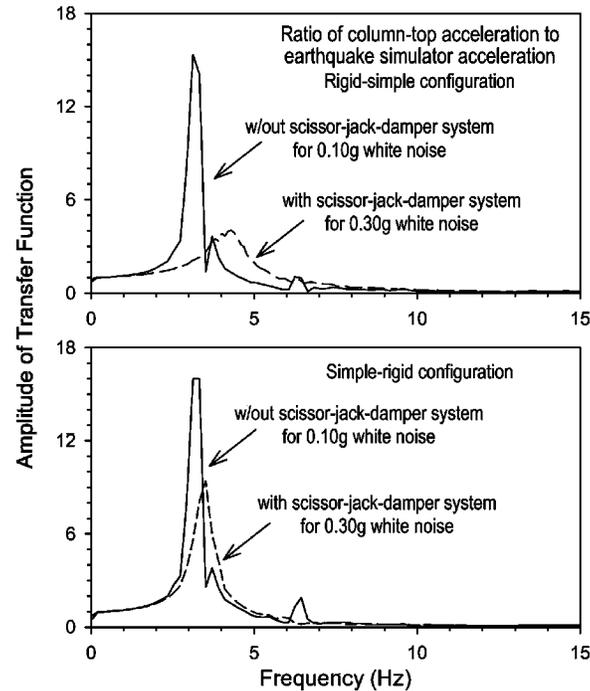
Figure 9. Amplitude of transfer function of model structure with *rigid-simple* and *simple-rigid* connections.

IDENTIFICATION OF DYNAMIC CHARACTERISTICS

The dynamic characteristics of the model (as depicted in Figures 5 and 6 with mass) were identified by exciting the structure on the earthquake simulator (with and without the scissor-jack-damper system) with stationary-banded white noise excitation. Transfer functions were then constructed as the ratio of the Fourier transform of the acceleration at the concrete mass-to-column joint to the Fourier transform of the base acceleration (obtained from east frame instruments). Note that the rigid concrete mass is simply connected to the top of the frames so that the movement of the concrete mass-to-column joint is effectively identical to the movement of the center of mass of the structure. Accordingly, the transfer function calculated on the basis of the description above may be used to obtain the dynamic characteristics of the model structure when it is represented as a single-degree-of-freedom system.

The amplitudes of the obtained transfer functions are presented in Figure 9. Note that the model structure was tested in two different configurations of the beam-to-column connections: rigid-simple, which amplifies the magnification factor, and simple-rigid, which causes an undesirable reduction of the factor. The amplitude of transfer functions reveals a simple relation that is characteristic of single-degree-of-freedom sys-

Table 1. Identified dynamic characteristics of model structure with and without scissor-jack-damper system

Beam-to-Column Connections	Configuration	Fundamental Frequency (Hz)	Damping Ratio
Rigid-Simple	No Dampers	3.2	0.035
	Scissor-Jack-Damper	4.0	0.130
Simple-Rigid	No Dampers	3.2	0.031
	Scissor-Jack-Damper	3.5	0.055

tems. Accordingly, the frequency and damping ratio on the basis of the assumption of linear elastic and linear viscous behavior may be easily determined. They are presented in Table 1 for each of the four tested configurations.

An observation to be made in the results of Table 1 and Figure 9 is the significant difference in the added damping in the two configurations of frames, of which the origin has been previously explained. Another important observation is the significant stiffening of the structure, marked by the increase in frequency. For the rigid-simple configuration, the increase in frequency from 3.2 to 4.0 Hz is significant and consistent with the approximately 60 percent increase in stiffness of the frame observed in testing under imposed displacement. This increase in frequency is the result of viscoelastic behavior caused by frame and energy dissipation assembly deformations under the action of the damping forces.

EARTHQUAKE SIMULATOR TESTING

The model structure was tested on the earthquake simulator in its rigid-simple beam-to-column connection configuration (see Figure 6). It was subjected to several ground motions, which were scaled in time by a factor of $\sqrt{2}$ in accordance with the model's length scale factor. The data acquisition system consisted of accelerometers, displacement transducers and load cells, which measured the response of the frame as well as the motion of the earthquake simulator. The instrumentation scheme was similar to that of the previously tested toggle-brace system, which can be found in Constantinou et al. (1997).

The ground motions used in the earthquake simulator testing included the 1940 El Centro, component S00E; 1952 Taft, component N21E; 1971 San Fernando at Pacoima Dam, components S16E and S74W; 1985 Mexico City at SCT, component N90W; 1978 Miyagiken-Oki, component EW; 1968 Hachinohe, component NS; 1995 Kobe, component EW; 1994 Northridge records at Sylmar, component 90°; and Newhall, components 90° and 360°.

A summary of the earthquake simulator testing results for a sample of ground motions is presented in Table 2, where each record is denoted by the excitation name, component, and acceleration amplitude scale. For example, EL CENTRO S00E 50% implies that the record was component S00E of the El Centro earthquake, scaled in amplitude of acceleration to 50 percent of the actual value. Tabulated in Table 2 are peak values of the

Table 2. Peak response of model in earthquake simulator testing

Excitation	Peak earthquake simulator motion			Drift (mm)	Accel. (g)	Damper displ. (mm)	Damper force (kN)	Scissor damper	Magnification factor
	Displ. (mm)	Veloc. (mm/s)	Accel. (g)						
EL CENTRO S00E 50%	20.2	115.6	0.200	14.3	0.606	-	-	NO	-
EL CENTRO S00E 50%	20.7	112.1	0.187	3.1	0.240	4.9	4.44	YES	1.6–1.8
EL CENTRO S00E 100%	41.5	219.7	0.340	6.5	0.459	10.8	8.66	YES	1.7–1.9
TAFT N21E 100%	21.8	103.5	0.156	7.3	0.336	-	-	NO	-
TAFT N21E 200%	43.6	207.6	0.316	7.6	0.560	11.7	9.77	YES	1.5–1.7
HACHINOHE NS 50%	25.1	108.0	0.127	8.5	0.378	-	-	NO	-
HACHINOHE NS 100%	50.0	212.1	0.252	5.9	0.432	8.9	7.47	YES	1.5–1.6
HACHINOHE NS 150%	75.1	321.3	0.371	8.7	0.600	12.1	9.94	YES	1.5–1.7
MIYAGIKEN EW 100%	17.3	94.6	0.146	10.6	0.451	-	-	NO	-
MIYAGIKEN EW 200%	34.7	203.2	0.284	6.9	0.494	10.8	8.64	YES	1.5
MIYAGIKEN EW 300%	52.4	308.0	0.456	10.3	0.683	15.9	11.56	YES	1.5–1.6
MEXICO CITY N90W 100%	100.1	412.8	0.196	6.8	0.321	-	-	NO	-
MEXICO CITY N90W 100%	101.1	417.5	0.199	3.2	0.192	6.4	2.40	YES	1.9–2.0
SYLMAR 90 25%	24.9	115.6	0.165	8.6	0.385	-	-	NO	-
SYLMAR 90 75%	76.2	317.5	0.413	7.8	0.561	13.0	9.87	YES	1.5–1.8
NEWHALL 360 25%	29.6	153.7	0.188	10.0	0.450	-	-	NO	-
NEWHALL 360 50%	60.0	298.5	0.414	7.2	0.534	12.4	9.36	YES	1.6–1.7
NEWHALL 90 25%	17.6	105.4	0.171	7.2	0.315	-	-	NO	-
NEWHALL 90 50%	35.8	203.2	0.402	9.0	0.655	14.9	10.04	YES	1.5–1.7
PACOIMA S74W 50%	27.9	219.4	0.486	9.0	0.689	15.7	12.27	YES	1.6–1.7
PACOIMA S16E 50%	74.4	307.6	0.505	9.5	0.670	15.5	11.81	YES	1.6
KOBE EW 40%	28.6	232.7	0.269	7.6	0.556	11.9	9.75	YES	1.5

earthquake simulator displacement, velocity and acceleration, and peak frame response in terms of drift (displacement of the beam-to-column joint with respect to the simulator), beam-to-column joint acceleration, damper displacement, and damper force. The peak frame output values are the average of the two quantities measured at east and west frames. The two values differ slightly due to accidental asymmetry caused by slight variations in stiffness of the two frames, and in damper properties.

The table also provides information on the measured range of values of the magnification factor for positive and negative directions of drift. As noted earlier, the magnification factor is dependent on the direction of movement due to changes in the geometry of the scissor-jack system. Measured values of the magnification factor lie in the range of 1.5 to 2.0 and are dependent on the excitation type. By comparison, the theoretical value is 1.8, whereas values measured in the testing of the frame under imposed harmonic displacement varied between 1.6 and 1.9.
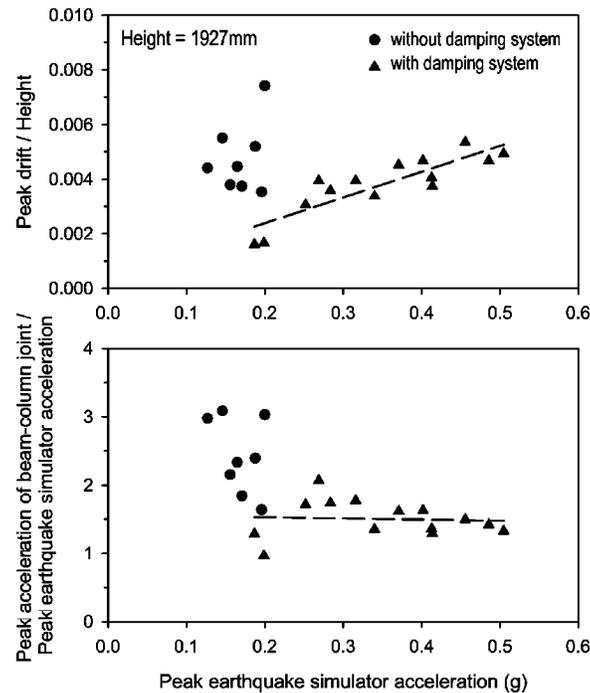
Figure 10. Peak response of model structure as a function of peak earthquake simulator acceleration: peak drift ratio (top) and normalized peak structural acceleration (bottom).

The results of Table 2 clearly demonstrate that the scissor-jack system operates as an effective damping system. Drift is substantially reduced. For example, observe the results in the El Centro motion. Without the scissor-jack system, the structure (which is essentially elastic with damping ratio of about 0.04) undergoes drift of 14.3 mm. The damped structure undergoes less than half that drift when excited by the El Centro motion scaled up by a significant amount. Interestingly in this case of elastic response, the peak-recorded acceleration is also smaller in the damped structure despite the stronger input. Similarly, the reader may want to compare the responses of the undamped and damped structures in the Mexico City motion. For the same input, the damped structure undergoes 50 percent lesser drift and 40 percent lesser acceleration.

A comparison of the performances of the structure without and with the damping system is presented in Figure 10 (using circular and triangular symbols, respectively), where the recorded peak drift ratio (peak drift—from Table 2—divided by the height of the tested structure) and normalized peak structural acceleration (peak acceleration of beam-to-column joint divided by peak earthquake simulator acceleration—both from Table 2) are plotted against the peak earthquake simulator acceleration. The latter may be regarded as representative of the intensity of the seismic excitation given the low period of the tested model. The benefits offered by the damping system are clearly evident in this figure: lower drift and lower acceleration for a given intensity of seismic excita-

tion. These benefits are typical of what damping systems may offer—the intent in showing these graphs being to demonstrate the equivalence of the scissor-jack-damper configuration to more conventional configurations.

Of interest is to discuss the effect of the stiffening of the structure on the reduction of response. The reduction in displacement response is certainly the combined result of stiffening of the structure and of increased damping. However, the reduction of acceleration response is primarily the result of increased damping. It should be noted that the model structure is stiff with a fundamental period that falls within the acceleration-sensitive region of the spectrum for all of the earthquake motions used in the testing, for which, reductions in period (stiffening) do not result in reduction of acceleration.

ANALYTICAL PREDICTION OF RESPONSE HISTORY

Dynamic analysis of the tested structure was performed using the computer program SAP2000 (Computers and Structures, Inc. 2000). This program is suitable for modeling structures that are primarily linear elastic, but may have a number of predefined nonlinear elements. That is, geometric nonlinearities and yielding frame action are not taken into account. The program was thus expected to replicate the dynamic behavior of the structure under the assumption of small deformations. While modeling of the structure was rather direct, it is beneficial to include a few details herein. The dampers were modeled as nonlinear viscous elements (using the **Nllink** element, **damper** property) with force-velocity relation given by $F_D = C_{No} \cdot \dot{u}_D{}^\alpha$ with parameters $C_{No} = 137.3$ N-(s/mm)$^\alpha$, and $\alpha = 0.76$, to simulate their behavior for a large range of damper velocities. In addition, artificial rotational springs were introduced at the joints where the scissor-braces and the damper were connected. These connections were not true pins so that the connections exhibited a finite amount of fixity, which slightly limited the rotation capacity of the joints.

Sample comparisons of experimental results to analytical predictions are presented in Figure 11 for El Centro S00E 100% and Sylmar 90 100% records. As evident in the figure, the analytical model is well capable of capturing significant characteristics of the behavior of the system such as the stiffening effect (evident by the matching frequency contents of the experimental and analytical response histories) and peak values of drift and acceleration. Also, the analysis tended to slightly overestimate the damper displacements and forces. It appears that the observed discrepancies in the calculated and measured responses of the dampers are due to geometric nonlinearities in the scissor-jack-damper system that cannot be accounted for in the SAP2000 analysis.

SIMPLIFIED ANALYSIS

Response history analysis represents the best means of calculating the seismic response of a structure with the scissor-jack system. Illustrated in Figure 12a is the complete structural representation of the tested model that was used in the response history analysis reported in the previous section with the exception that the damper is linear viscous as described by Equation 3. This representation may be simplified for ease in the dynamic analysis by replacing the scissor-jack assembly by an equivalent spring and dashpot system as shown in Figure 12b. Note that the quantity K_a represents the stiffness
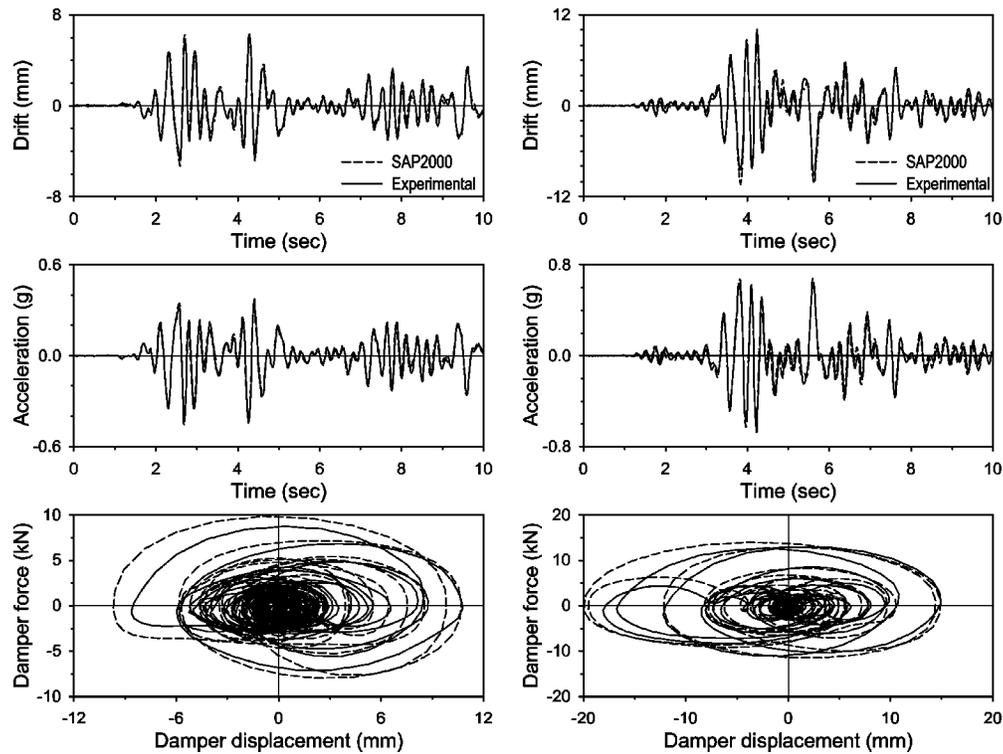
Figure 11. Comparison of analytical (SAP2000) and experimental response of model structure with rigid-simple beam-to-column connections for: 1940 El Centro earthquake, PGA=0.34 g (left), and 1994 Northridge earthquake, Sylmar record, component 90, PGA=0.60 g (right).

of the assembly only, which is typically very large. It is determined by the procedure illustrated in Figure 12b. Note that in the calculation of stiffness, the damper is considered "locked" so that it acts as a spring with stiffness equal to that of the oil column in the damper. The stiffness is given by $A_r^2 \cdot B/V$, where A_r is the piston rod area, V is the effective volume of fluid, and B is its bulk modulus. In the case of the damper in the tested model, the stiffness of the locked damper was represented by a steel element having a diameter of 10 mm and length equal to that of the damper.

Simplified analysis is based on the premise that a linear elastic and proportional linear viscous representation of the structural system produces estimates of the seismic response that are of acceptable accuracy. A discussion on the subject may be found in Hanson and Soong (2001); several examples of application of simplified methods of analysis and evaluation of the accuracy of the methods may be found in Ramirez et al. (2000). Herein, we concentrate on the prediction of the fundamental period and associated damping ratio of the tested model using simplified methods of analysis described by Equations 17 and 20.
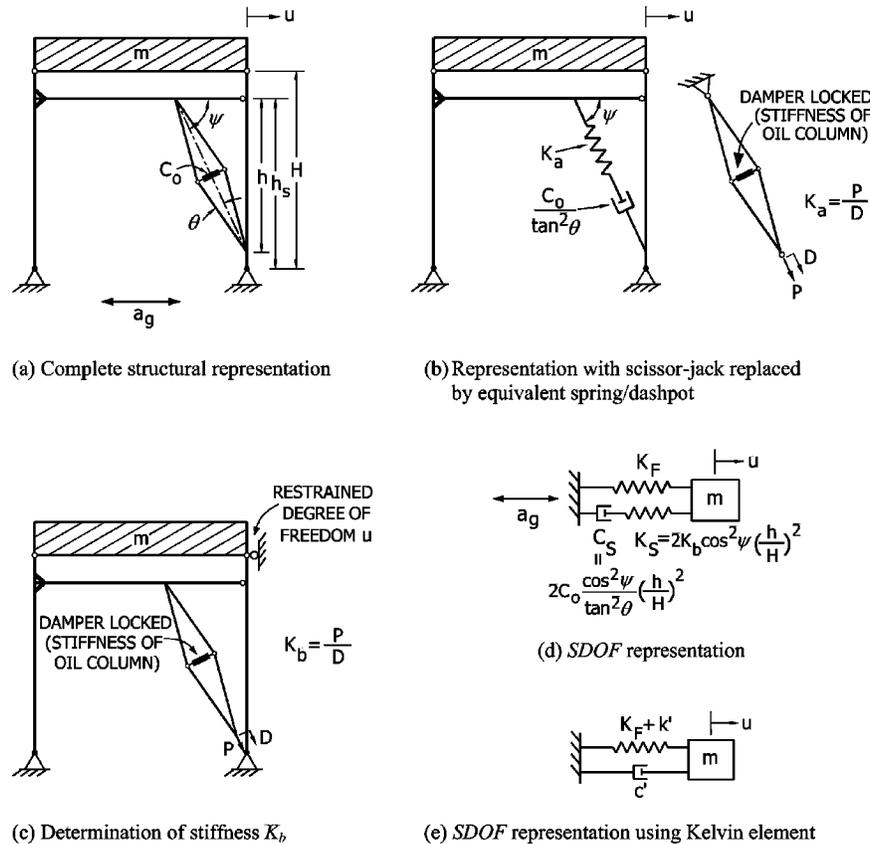
(a) Complete structural representation

(b) Representation with scissor-jack replaced by equivalent spring/dashpot

(c) Determination of stiffness K_b

(d) *SDOF* representation

(e) *SDOF* representation using Kelvin element

Figure 12. Representation of structure for simplified analysis.

The tested model is simple in the sense that it essentially is a single-degree-of-freedom system undergoing elastic deformations. Yet, application of the simplified methods for predicting the period and damping ratio are complicated by the effect of the deformations of the frame under the action of the damping forces, which results in a substantial increase in stiffness. Prediction of this increase in stiffness is important in the application of simplified analysis.

Figure 12c illustrates the procedure for calculating stiffness parameter K_b. Half of the structure (due to symmetry) is analyzed with the lateral degree of freedom restrained, the scissor-jack assembly disconnected from the column and a displacement D applied along the axis of the scissor-jack. The force P needed to produce displacement D is calculated and the stiffness parameter is computed as $K_b = P/D$. This stiffness is simply related to the added stiffness provided by the energy dissipation assembly. Stiffness K_b was calculated to be 34.5 kN/mm.

Shown in Figure 12d is a single-degree-of-freedom representation of the model structure. In this representation, K_F is the lateral stiffness of the frame, exclusive of the

energy dissipation system, and K_S and C_S are the stiffness and damping constant, respectively, contributed by the scissor-jack-damper system (two scissor-jacks) inclusive of the effect of its interaction with the frame. These parameters are given by

$$K_S = 2 \cdot K_b \cdot \cos^2 \psi \cdot \left(\frac{\phi_{r1}}{\phi_1}\right)^2 \approx 2 \cdot K_b \cdot \cos^2 \psi \cdot \left(\frac{h}{H}\right)^2 \tag{22}$$

$$C_S = 2 \cdot \frac{C_o \cdot \cos^2 \psi}{\tan^2 \theta} \cdot \left(\frac{\phi_{r1}}{\phi_1}\right)^2 \approx 2 \cdot \frac{C_o \cdot \cos^2 \psi}{\tan^2 \theta} \cdot \left(\frac{h}{H}\right)^2 \tag{23}$$

where ϕ_{r1} is the relative modal horizontal displacement of the two ends of the scissor-braces and ϕ_1 is the modal displacement of the center of mass of the concrete block. For the model structure, $\phi_{r1}/\phi_1 \approx h/H$, where heights h and H are identified in Figures 4 and 12a.

Analysis of the single-degree-of-freedom representation of Figure 12d is itself complicated, given the viscoelastic nature of the system. For example, calculation of the period and damping ratio requires complex eigenvalue analysis (Constantinou and Symans 1992). Simplified analysis would require a further step of replacing the Maxwell element in Figure 12d by an equivalent Kelvin element of stiffness k' and damping constant c' (Constantinou et al. 1998), as shown in Figure 12e, where

$$k' = \frac{C_S \cdot \tau \cdot \omega^2}{1 + \tau^2 \cdot \omega^2} \tag{24}$$

$$c' = \frac{C_S}{1 + \tau^2 \cdot \omega^2} \tag{25}$$

$$\tau = \frac{C_S}{K_S} = \frac{C_o}{\tan^2 \theta \cdot K_b} \tag{26}$$

Parameter $\omega = 2 \cdot \pi / T_1$ is the frequency of vibration of the damped structure. Note that parameter τ is the relaxation time, which also appears in Equations 20 and 21.

On the basis of the representation shown in Figure 12e, the period, T_1, and damping ratio, β_1, of the damped structure are

$$T_1 = 2 \cdot \pi \cdot \left[\frac{m}{K_F + k'}\right]^{1/2} = T_1' \cdot \left[1 - \frac{4 \cdot \pi \cdot \tau \cdot \beta_1}{T_1}\right]^{1/2} \tag{27}$$

$$\beta_1 = \frac{c' \cdot T_1}{4 \cdot \pi \cdot m} = \frac{C_o \cdot \cos^2 \psi \cdot T_1}{2 \cdot \pi \cdot m \cdot (1 + \tau^2 \cdot \omega^2) \cdot \tan^2 \theta} \cdot \left(\frac{h}{H}\right)^2 \tag{28}$$

where T_1' is the period of vibration of the structure exclusive of the energy dissipation system,

$$T_1' = 2 \cdot \pi \cdot \left[\frac{m}{K_F} \right]^{1/2} \tag{29}$$

Equations 27 and 28 are identical to Equations 20 and 17, respectively, for the model structure, with the exception that ϕ_{r1}/ϕ_1 appears instead of h/H.

For the purpose of performing calculations $C_o=40.0$ N-s/mm was used, a value which represents well the behavior of the dampers for velocities less than about 250 mm/s (see Figure 7). Equation 26 results in $\tau=0.046$ s. Period $T_1'=0.31$ s based on the model identification (frequency of 3.2 Hz). Moreover, $\phi_{r1}/\phi_1 \approx h/H = 0.68$ and Equations 27 and 28 are iteratively solved to result in $T_1=0.27$ s and $\beta_1=0.12$. Note that the period of 0.27 s corresponds to a frequency of 3.7 Hz, which is less than the identified value of 4.0 Hz (see Table 1) but sufficiently close for practical purposes. Also, the calculated damping ratio of 0.12 represents the added value supplied by the damping system. Since the inherent damping was of the order of 0.04, the total damping ratio is about 0.16. Identification of the structure showed a total damping ratio of 0.13 (see Table 1). Simplified analysis predicts well the dynamic properties of the model.

CONCLUSIONS

Scissor-jack-damper energy dissipation systems offer a new opportunity to apply damping systems. As the toggle-brace-damper system that preceded its development, the scissor-jack-damper system utilizes shallow trusses to magnify the damper displacement for a given interstory drift, and to magnify the damper force output delivered to the structural frame. The system thus extends the applicability of damping devices to cases of small interstory drifts, such as stiff structures under seismic loading and structures subjected to wind loading. Moreover, the scissor-jack damping system can be configured to allow for open space through its compactness and near-vertical installation, a feature that is often desired for architectural purposes.

This paper presented a theoretical treatment of the scissor-jack-damper system and experimental results that demonstrated its effectiveness. Testing of a half-scale steel model structure on the earthquake simulator indicated a significant increase in the damping ratio, accompanied with reduction in drift and acceleration responses. The scissor-jack-damper system also caused stiffening of the structure, marked by the increase in frequency. This viscoelastic behavior occurred as a result of frame and energy dissipation assembly deformations under the action of damping forces.

The response of the model structure was reproduced analytically with acceptable accuracy by response history analysis. The analytical model satisfactorily captured significant characteristics of the model such as the stiffening effect, and peak values of drift and acceleration. In addition, the application of simplified analysis methods for predicting period and damping ratio of the model structure was presented. Simplified analysis requires a proper representation of the increase in stiffness of the structure due to the damping system. Results of this analysis were in close agreement with those of the experiments.

ACKNOWLEDGMENTS

REFERENCES

Applied Technology Council (ATC), 1997. *NEHRP Guidelines for the Seismic Rehabilitation of Buildings*, (*FEMA 273 Guidelines* and *FEMA 274 Commentary*), prepared for the Building Seismic Safety Council, published by the Federal Emergency Management Agency, Washington, DC.

Computers and Structures Inc., 2000. SAP2000: *Static and Dynamic Finite Element Analysis of Structures (Nonlinear Version 7.40)*, Computers and Structures Inc., Berkeley, CA.

Constantinou, M. C., 2000. Damping systems for structural design and retrofit, *Presentation, EERI 52nd Annual Meeting*, St. Louis, MO.

Constantinou, M. C., and Şigaher, N., 2000. Energy dissipation system configurations for improved performance, *Proceedings of the 2000 Structures Congress & Exposition*, ASCE, Philadelphia, PA.

Constantinou, M. C., Soong, T. T., and Dargush, G. F., 1998. *Passive energy dissipation systems for structural design and retrofit*, Monograph No. 1, Multidisciplinary Center for Earthquake Engineering Research, Buffalo, NY.

Constantinou, M. C., and Symans, M. D., 1992. *Experimental and Analytical Investigation of Seismic Response of Structures with Supplemental Fluid Viscous Dampers, Technical Report NCEER-92-0032*, National Center for Earthquake Engineering Research, Buffalo, NY.

Constantinou, M. C., Tsopelas, P., and Hammel, W., 1997. Testing and modeling of an improved damper configuration for stiff structural systems, Center for Industrial Effectiveness, University at Buffalo, SUNY, Buffalo, NY, ⟨*http://civil.eng.buffalo.edu/users_ntwk/*⟩.

Constantinou, M. C., Tsopelas, P., Hammel, W., and Şigaher, A. N., 2000. New configurations of fluid viscous dampers for improved performance: *Proceedings of the Passive Structural Control Symposium 2000*, Tokyo Institute of Technology, Yokohama, Japan.

Constantinou, M. C., Tsopelas, P., Hammel, W., and Şigaher, A. N., 2001. Toggle-brace-damper seismic energy dissipation systems, *J. Struct. Eng.* **127** (2), 105–112.

Federal Emergency Management Agency (FEMA), 2000. *NEHRP Recommended Provisions for Seismic Regulations for New Buildings and Other Structures, (FEMA 368)*, Washington, DC.

Hanson, R. D., and Soong, T. T., 2001. *Seismic Design with Supplemental Energy Dissipation Devices*, Monograph No. 8, Earthquake Engineering Research Institute, Oakland, CA.

Ramirez, O. M., Constantinou, M. C., Kircher, C. A., Whittaker, A. S., Johnson, M. W., Gomez, J. D., and Chrysostomou, C. Z., 2000. *Development and Evaluation of Simplified Procedures for Analysis and Design of Buildings with Passive Energy Dissipation Systems, Technical Report MCEER-00-0010, Revision 1*, Multidisciplinary Center for Earthquake Engineering Research, Buffalo, NY.

Soong, T. T., and Dargush, G. F., 1997. *Passive Energy Dissipation Systems in Structural Engineering*, John Wiley & Sons Ltd., London (UK) and New York (USA).

Veletsos, A. S., and Ventura, C. E., 1986. Modal analysis of non-proportionally damped linear systems, *Earthquake Eng. Struct. Dyn.* **14**, 217–243.

Whittaker, A. S., and Constantinou, M. C., 1999a. Advances in supplemental damping systems for civil infrastructure, *Proceedings of the VIIth Mexican Conference on Earthquake Engineering*, Morelia, Mexico.

Whittaker, A. S., and Constantinou, M. C., 1999b. Supplemental damping for new and retrofit construction, *Revista de Ingenieria Sismica, Vol. 61*, Sociedad Mexicana de Ingenieria Sismica A. C., Mexico City.

Whittaker, A. S., and Constantinou, M. C., 2000. Fluid viscous dampers for building construction, *Proceedings of the Passive Structural Control Symposium 2000*, Tokyo Institute of Technology, Yokohama, Japan.